Journal of the American College of Cardiology
© 2002 by the American College of Cardiology Foundation
Published by Elsevier Science Inc.
Vol. 39, No. 8, 2002
ISSN 0735-1097/02/$22.00
PII S0735-1097(02)01754-0

EXPERIMENTAL STUDIES

In Vivo Noninvasive Detection and Age Definition of Arterial Thrombus by MRI

Roberto Corti, MD,*† Julio I. Osende, MD,*† Zahi A. Fayad, PHD,†‡
John T. Fallon, MD, PHD, FACC,†§ Valentin Fuster, MD, PHD, FACC,† Gabor Mizsei, MS,†‡
Elisha Dickstein, BA,* Burton Drayer, MD,‡ Juan J. Badimon, PHD, FACC*†
New York, New York

OBJECTIVES The purpose of this study was to evaluate the potential of magnetic resonance (MR) to detect arterial thrombotic obstruction and define thrombus age.

BACKGROUND Arterial thrombi underlie the clinical consequences of atherosclerosis and are not reliably detected by current noninvasive diagnostic techniques.

METHODS Carotid thrombi were induced in swine (n = 7) by arterial injury. Serial high-resolution in vivo MR images were obtained using black-blood T1-weighted (T1W) and T2-weighted (T2W) sequences in a clinical 1.5T MR system at 6 h, 1 day and at 1, 2, 3, 6 and 9 weeks. At each time point one animal was sacrificed and the occluded carotid artery processed for histopathology. Thrombus signal intensity (SI) was normalized to that of the adjacent muscle. Thrombus age was assessed based on MR appearance by two blinded independent observers.

RESULTS Thrombus appearance and relative SI revealed characteristic temporal changes in multicontrast-weighted MR images, reflecting histologic changes in the composition. Acute thrombus appeared very bright on the T2W images, facilitating the detection. Signal intensity was 197 ± 25% at 6 h, peaking at 1 week (246 ± 51%), reaching a plateau by 6 weeks (120 ± 15%). At six weeks, complete thrombus organization was confirmed histologically. The T1W images had similar pattern with lower SI than T2W. Age definition using visual appearance was highly accurate (Pearson's chi-square with 4 df ranging from 96 to 132 and Cohen's kappa at 0.81 to 0.94). Agreement between observers was substantial (Pearson chi-square with 4 df = 91.5, kappa = 0.79).

CONCLUSIONS Magnetic resonance imaging is a promising tool to noninvasively detect arterial thrombosis. Measurement of SI and the characteristic visual appearance of the thrombus have the potential to define thrombus age. (J Am Coll Cardiol 2002;39:1366–73) © 2002 by the American College of Cardiology Foundation

Despite advances in our understanding of the pathogenesis (1,2), newer treatment modalities and increased preventive efforts, thrombotic complications of atherosclerosis remain the leading cause of morbidity and mortality in Western society and are an emerging epidemic in developing countries (3). Disruption of atherosclerotic plaques is known to initiate thrombus formation leading to thrombotic and thromboembolic events (4–6). Therefore, the detection of evolving arterial thrombus noninvasively can have significant diagnostic and therapeutic implications. Although different imaging methods are now clinically available for the diagnosis of luminal narrowing, arterial occlusion and intramural hematoma (7), arterial thrombi are not reliably detected by current diagnostic techniques. Angioscopy (8,9), for instance, is invasive and not widely available. Intravascular ultrasound and angiography are invasive and use indirect and nonsensitive criteria for thrombus detection.

Among the different imaging modalities, magnetic resonance (MR) is emerging as the potential leading noninvasive in vivo imaging modality for atherosclerosis (10). Magnetic resonance differentiates tissue components on the basis of biophysical and biochemical parameters such as chemical composition, water content, physical state, molecular motion or diffusion. We and others have previously reported that MR imaging allows accurate quantification and characterization of atherosclerotic lesions in various arterial beds (11–16). We have reported an anecdotal MR observation showing time-dependent signal changes in the thrombosed false lumen of an aortic dissection in an atherosclerotic rabbit (17). Recently, MR was used to image thrombus formation in the abdominal aorta in the atherosclerotic rabbit model using a T2-weighted (T2W) MR sequence (18).

Several groups have previously highlighted the importance of gradient echo MR imaging in the study of cerebral hematoma and venous thrombosis (19,20). Based on our ongoing experience in MR plaque imaging, we specifically decided to test multicontrast fast spin echo sequences—which are commonly used for high-resolution MR imaging of atherosclerotic plaques—for thrombus visualization and characterization of thrombus age.

From the *Cardiovascular Biology Research Laboratory, †Cardiovascular Institute, Departments of ‡Radiology and §Pathology, Mount Sinai Medical Center, New York, New York. Supported, in part, by grants from NIH SCOR HL54469 (V. F. and J. J. B.) and the Swiss National Research Foundation (R. C.).

Manuscript received October 15, 2001; revised manuscript received January 17, 2002, accepted January 28, 2002.

Abbreviations and Acronyms

df	= degree of freedom
LL	= Log Likelihood
MR	= magnetic resonance
RBC	= red blood cell
SI	= signal intensity
TE	= echo time
TR	= repetition time
T1W	= T1-weighted
T2W	= T2-weighted
2IR-FSE	= double inversion recovery fast spin echo

We now report the serial in vivo imaging and characterization of arterial thrombosis in swine using a clinical MR system.

The ability to noninvasively detect thrombotic material in the arterial circulation may improve our knowledge of pathophysiology in the field of atherothrombosis and may permit quantitative monitoring of thrombus growth and assessment of treatment efficacy over time. Moreover, the ability to reliably differentiate between recent and old thrombi may give relevant information for patients' risk stratification and could allow tailoring of therapeutic approaches.

METHODS

Model of artery thrombosis in porcine carotid arteries. Yorkshire albino swine (n = 7, 35 kg) were selected for this study. Anesthetic and surgical preparations for the carotid injury were performed as previously described (21). Thrombus formation in the common carotid artery was performed by modification of a previously reported technique (21). In brief, we induced: 1) deep arterial injury by 4 to 6 balloon inflations (Titan, Cordis Corp., Miami, Florida) to 1.5 to 2 times the normal lumen diameter to a maximum of 15 atms, followed by, 2) de-endothelialization by pullback of the inflated balloon to facilitate thrombus adhesion, and 3) reduction of blood flow by subocclusive inflation of the balloon proximal to the injured segment until occlusion or subocclusion was confirmed by angiography (30 to 45 min). After the procedure, animals were transferred to the MR and allowed to recover.

The handling, maintenance and care of the animals, as well as all the procedures performed in this protocol, were approved by the Mount Sinai School of Medicine Animal Management Program and followed the AHA Guidelines for Animal Research.

In vivo MR imaging. The injured artery and the contralateral normal carotid artery were imaged shortly after thrombus induction (≤6 h), as well as at day 1 and weeks 1, 2, 3, 6 and 9. Anesthesia was performed as previously reported (22). In brief, before the MR study, the pigs were premedicated with ketamine 15 mg/kg intramuscularly (Ketaset, Fort Dodge Animal Health, Overland Park, Kansas) and anesthesia induced with intravenous propofol 10 mg/kg (Diprivan 1%, Zeneca Pharmaceuticals, Wilmington, Delaware) followed by continuous infusion of propofol 10 to 15 mg/kg/h. Animals were intubated and mechanically ventilated with a MR compatible ventilator (pneuPAC, Broomall, Pennsylvania), were placed supine in the magnet, and a customized two-element phased-array surface coil was placed on the neck. Magnetic resonance imaging was performed using a Signa clinical 1.5T magnet (GE Medical Systems, Mount Prospect, Illinois) as previously described (22) using modified fast spin echo black-blood multicontrast sequences. After initial gradient echo series to localize the aortic arch and the carotid artery, noncontrast MR angiography was performed to localize the obstruction with time-of-flight technique. All subsequent imaging used the double inversion recovery fast spin echo (2IR-FSE) sequence for T2W and T1-weighted (T1W) images. The 2IR-FSE allows nulling of the signal from the flowing blood and is known as black-blood MR imaging. Contiguous cross-sectional images were obtained perpendicular to the long axis of the neck. The T1W and T2W images were acquired with a repetition time (TR) and echo time (TE) of 700 ms/11 ms and 2,000 ms/42 ms, respectively. Further MR imaging parameters included: receiver bandwidth ±62.5 Hz; echo train length 32; 4.4 ms echo spacing; field-of-view 12 × 12 cm; matrix 256×256 (zero-filled interpolated to 512×512, in order to reduce the partial-volume effects in imaging pixels [23]); and 3-mm slice thickness and two signal averages. High-resolution black-blood MR images of carotid arteries were obtained with an in-plane resolution of 470 × 470 μm^2. The addition of a fat suppression pulse allowed an easier detection of the thrombus. The choice of TR and TE parameters was based on ex vivo and in vivo studies on plaque imaging, as previously reported (12,14,16,22,24).

Euthanasia and specimen fixation. For histopathologic evaluation of thrombus composition and correlation of the thrombus dimensions with MR imaging, one animal was sacrificed at each imaging time point. Animals were sacrificed within the 12 h after the MR examination. For the acute time points (6 h and 1 day), the animals were sacrificed immediately after MR imaging.

To avoid postmortem thrombus formation, heparin (100 IU/kg) was administered 10 min before euthanasia by injection of Sleepaway (Fort Dodge Animal Health). After euthanasia the carotid arteries were gently rinsed in 0.01 mol/l phosphate buffer saline and transferred to cold (4°C) 4% paraformaldehyde solution. Serial cross-sections of the carotid arteries were cut at 3-mm intervals matching corresponding MR images (described in the following text) and kept in fresh fixative. Specimens were then paraffin-embedded, cut into 5-μm sections and stained with combined Masson's elastin technique.

An independent observer blinded to the age of thrombus and to the MR results performed the histologic analysis of thrombus composition.

JACC Vol. 39, No. 8, 2002
April 17, 2002:1366–73

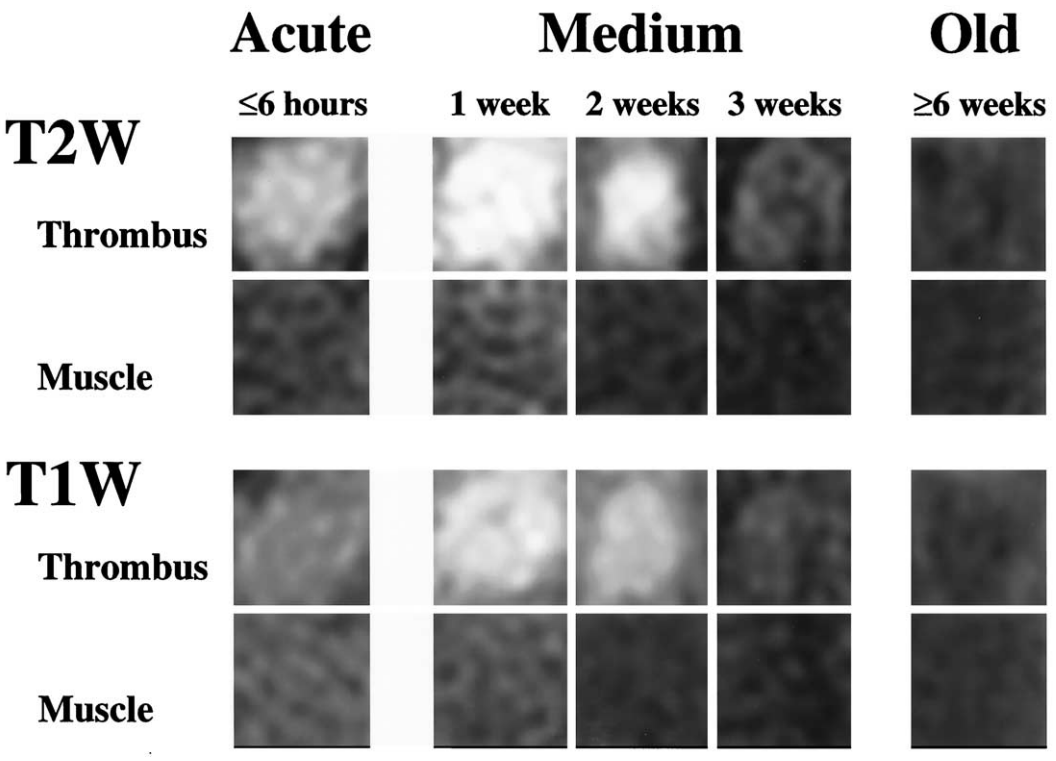

Figure 1. Representative T2-weighted (T2W) and T1-weighted (T1W) axial magnetic resonance images of the thrombus and adjacent muscle (used as reference) at different time points after thrombus induction were selected to create a reference table for visual comparison. This figure was used as reference for signal intensity analysis by the two independent observers.

Data analysis. The MR images were transferred to a Macintosh computer for analysis. The histopathologic sections were digitized to the same computer from a camera (Sony, 3CCD Video Camera, Japan) attached to a Zeiss Axioskop (Carl Zeiss, Germany) light microscope. The MR images were then matched with corresponding histopathologic sections of thrombotic carotid artery specimens (n = 56). Co-registration was carefully performed utilizing one or more anatomic landmark structures, including the origin of the carotid artery, the bifurcation and arterial branches. Cross-sectional area of the thrombus was determined for both MR images and histopathology by manual tracing using ImagePro Plus (Media Cybernetics, Silver Spring, Maryland). Two blinded investigators performed the analysis. To define intraobserver and interobserver variability, a random subset of thrombosed carotid arteries segment MR images (n = 25) and corresponding histopathology sections were re-analyzed and the intraclass correlation coefficients determined.

Changes in MR signal intensity (SI). All MR images obtained were analyzed for the presence or absence of thrombotic occlusions. As thrombus composition changes through time, we assessed the intrinsic MR properties of the thrombus by measuring the relative SI to the reference muscle using the formula SI (%) = 100·[(SI thrombus) / (SI muscle)] on the T1W and T2W images. The immediately adjacent muscle tissue, equidistant from the surface phased-array MR coil, was selected as standard reference. The SI of the thrombus was assessed in its lengthwise central portion excluding the proximal and distal edges. Given that thrombus growth and dissolution are a dynamic process mainly located at the thrombus head and tail, the central portion of the thrombus may better reflect the age of the induced thrombus. The individual values of SI measurements of 5 to 10 contiguous images for each MR study sequence were averaged, and the mean SI at each time point was plotted over time.

Thrombus age. To visually characterize thrombus age, we used the appearance of the SI of the thrombus compared with the adjacent muscle. This allowed us to define arbitrary visual criteria (Fig. 1) to determine thrombus age. Seventy-three representative thrombus images were selected from different time points for visual definition of thrombus age. For each thrombus image, T2W and corresponding T1W images were printed on a separate glossy paper. The level of the contrast was kept uniform for all the images. Two independent observers blinded to thrombus age and to the pig identity performed the visual analysis of the thrombus using the previously defined visual criteria. The observers were asked to localize the thrombus and categorize the age (acute, 6 h; medium, 1 to 3 weeks; old, ≥6 weeks).

Data and statistics. Continuous data are expressed as mean ± SD. The data were described and prepared for analysis using SYSTAT (SPSS Inc., 2000, Chicago, Illinois), whereas the multilevel modeling was done with the SAS Proc Mixed procedure (Littell, Milliken, Stroup &

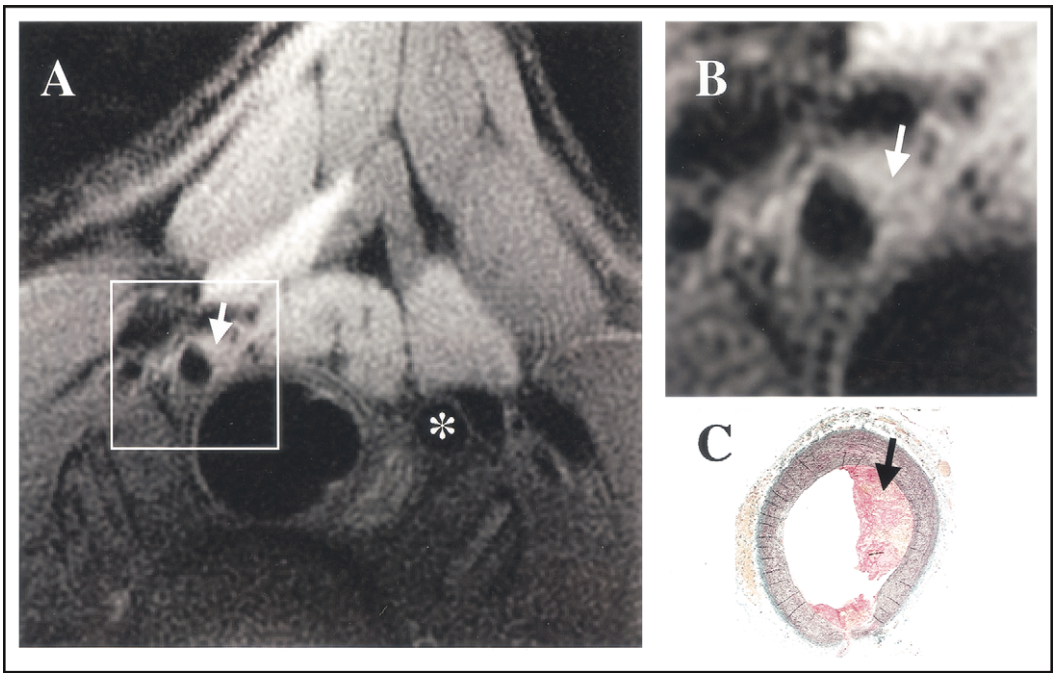

Figure 2. Axial black-blood T2-weighted magnetic resonance image showing a 24-h old mural, eccentrically shaped thrombus **(A)**, magnified 2.5× in **B.** The **arrows** indicate the thrombus in the injured right carotid artery, and the **asterisk** indicates the noninjured left carotid artery. The signal from the flowing blood in the lumen is black due to the double-inversion preparatory pulses. The corresponding histologic section is shown in **C.** The appearance of the thrombus on the magnetic resonance image correlates closely with the matched histologic section shown in **C.**

Wolfinger, 1996, SAS Institute, Cary, North Carolina). The multilevel modeling procedures were used to estimate and test the overall time trends in the data while adjusting for the incomplete and nested (dependent) nature of the data. Thus, the image data were both nested within pig, and not all pigs contributed data at each time point. We adjusted the orthogonal polynomial coefficients to represent the trends in the data to reflect the unequal spacing of the intervals. The accuracy in the visual definition of thrombus age is reported using Pearson's chi-square with degree of freedom (df) and Cohen's kappa. A $p < 0.05$ was considered as statistically significant.

RESULTS

Carotid artery thrombus was successfully induced in all the animals by this modified balloon catheter-based injury model. Thrombus was occlusive in six cases and partially occlusive in one animal. Magnetic resonance angiography accurately localized the arterial obstruction and detected the presence of large collaterals but did not provide any information on the etiology of the obstruction.

In all animals, thrombotic and normal (contralateral) carotid arteries were identified correctly in the axial images using black-blood technique. Moreover, black-blood MR imaging clearly differentiated between total occlusion and subocclusion (Fig. 2).

Thrombus aging and MR SI. Thrombus MR imaging showed time-dependent changes on T2W and T1W images (Fig. 3). These changes reflected the thrombus organization, as shown by histologic analysis (as described in the following text). The statistical analysis of trends of the SI time course for both T1W and T2W images revealed a cubic pattern, which was highly significant even after correction for the different number of observations at each time point nested within the study (T1W images: SE = 7.02, t value = 7.2, $p < 0.0001$ and −2 Log Likelihood (LL) = 1315.9; T2W images: SE = 10.14, t value = 6.84, $p < 0.0001$ and −2 LL = 1361.3). The T2W images of the acute thrombus appeared hyperintense in the few hours after induction. The initial SI at 6 h was 197.3 ± 25%, peaked at 1 week to 246.41 ± 51% ($p < 0.0001$ vs. 6-h old) and progressively decreased to 119.5 ± 15% at 6 weeks and remained unchanged until 9 weeks (Fig. 4). Statistical analysis of the temporal changes of SI is summarized in Table 1. The T1W images showed a similar pattern of SI changes over time: 123.7 ± 16% at 6 h, 199.3 ± 39% at 1 week ($p < 0.01$ vs. 6-h old) and 126 ± 10% at 6 weeks. The relative SI intensity in T2W images was significantly higher than in T1W images, and the statistical significance was the strongest during the first three weeks after thrombus induction, supporting the use of T2W sequences for the detection of acute thrombi.

Thrombus age. Two independent observers blinded to thrombus age performed the visual analysis for age definition. Definition of thrombus age by MR, using the characteristic visual appearance on T2W and T1W images and direct comparison with Figure 1 was highly accurate. Both observers' classifications are significantly related to the true age of the thrombi. Observer #1 had a Pearson's chi-square with 4 df = 96.01, $p < 0.0001$, kappa = 0.81. Observer #2 had a Pearson's chi-square with 4 df = 132.25, $p < 0.0001$, kappa = 0.94. Agreement between observers was substan-

JACC Vol. 39, No. 8, 2002
April 17, 2002:1366–73

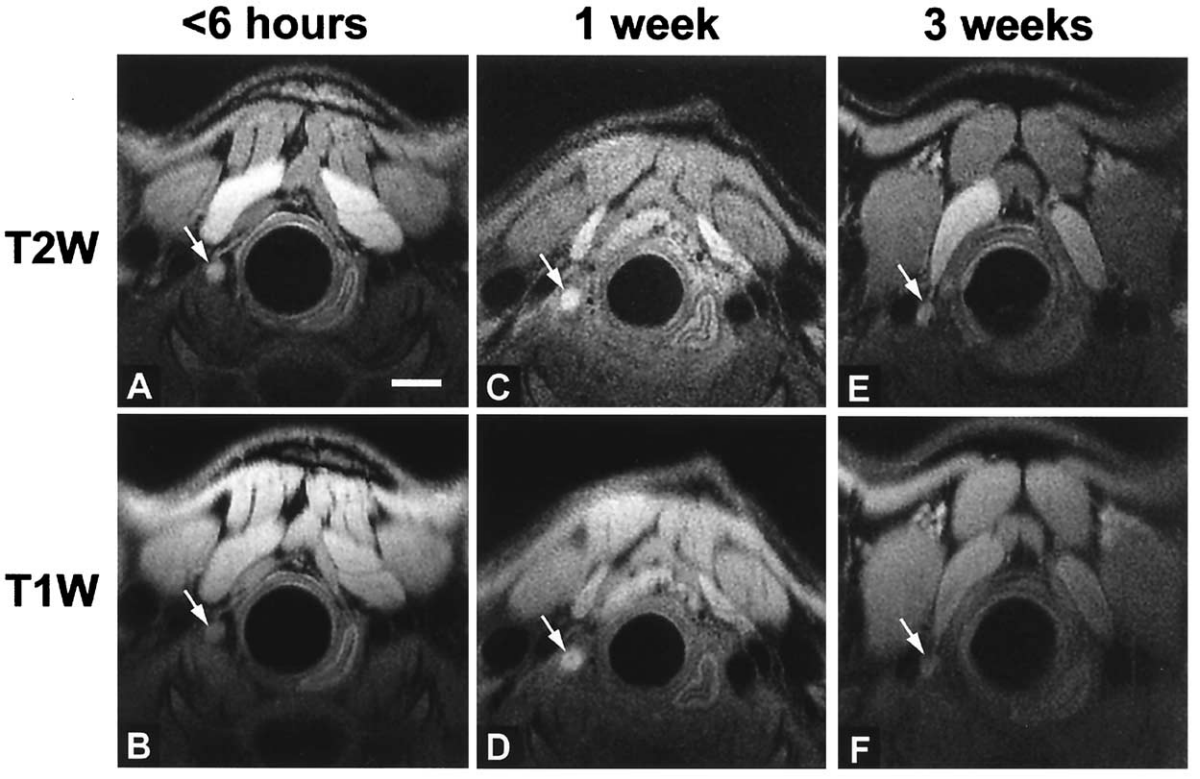

Figure 3. The thrombus revealed characteristic time-dependent changes in its appearance in T2-weighted (T2W) and T1-weighted (T1W) images in the sequential magnetic resonance (MR) scans reflecting the course of the signal intensity. Axial black-blood T2W **(A, C, E)** and T1W **(B, D, F)** MR images demonstrating the changes of the MR signal intensity of the thrombus over time. The difference in the MR signal between the thrombotic artery **(arrow)** and the adjacent muscle is particularly evident during the first three weeks. **Bar scale** = 1 cm.

tial: Pearson's chi-square with 4 df = 96.01, $p < 0.0001$, kappa = 0.79. Differentiation between acute and three-week-old thrombi was particularly difficult, reflecting comparable values of SI as reported in Figure 4. In contrast, acute and old (≥6-week-old) thrombi were easier to differentiate.

The sensitivity and specificity of the two independent observers for each of the three age categories (acute, medium and old) are given in Table 2.

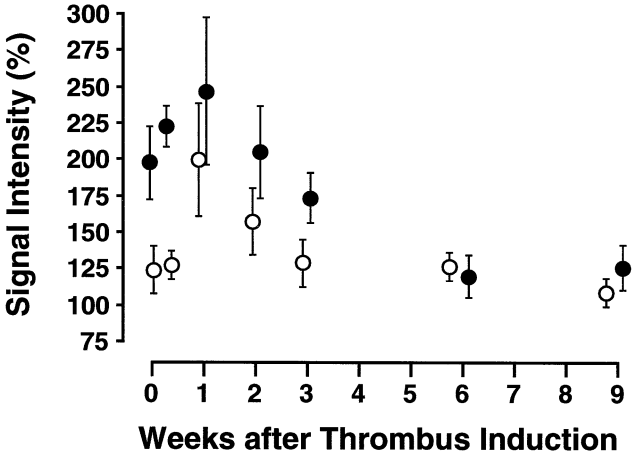

Figure 4. Thrombus signal intensity changes over time for both T1-weighted **(white circles)** and T2-weighted **(black circles)** images.

Histologic analysis of thrombi. The time-dependent changes in thrombus composition are shown in Figure 5. The composition reflects typical thrombus characteristics as described in histopathologic studies in humans. The acute thrombus (Fig. 5A) showed histopathologic characteristics of a fresh mixed, unorganized arterial thrombus mostly composed of platelets and fibrin mesh. Interestingly, the composition of the thrombus was not homogeneous; fibrin-rich areas were mixed with platelet-rich areas and sporadic areas of erythrocyte aggregates. Platelet-rich masses were densely packed and surrounded by layers of fibrin. Fibrin-rich areas were present mostly in the interface with the injured vessel, in particular where the thrombus was attached to the areas of exposed media. In addition, intact neutrophils and lines of Zahn were also observed. Twenty-four hours after thrombus induction, composition was histopathologically similar to acute thrombus. In fact, fibrin, red blood cells (RBCs) and platelet-rich areas were still very compact, and neutrophils appeared degranulated. At one week, granular platelets and/or poorly defined cellular material (probably cellular debris) were detected among fibrin strands (Fig. 5B, lower panel), but fibrin masses still appeared compacted (Fig. 5B, upper panel). At two weeks, initial fibrotic replacement was detected inside the thrombus with formation of layers of young connective tissue, whereas unresorbed fibrin and cellular debris was still present. At

Table 1. Statistical Analysis of the Temporal Changes for the T1W and T2W Data

	T1W				T2W			
	SE	t Value	p Value	−2LL	SE	t Value	p Value	−2LL
6 h–1 wk	3.90	−9.69	<0.0001	1,287.9	6.81	−3.86	0.0002	1,386.0
6 h–9 wk	6.46	−1.30	0.1946	1,357.2	8.87	2.32	0.0219	1,394.9
1 wk–9 wk	4.52	11.11	<0.0001	1,273.9	6.99	8.89	<0.0001	1,340.8

The degree of freedom (df) for the tests are 128 for T1-weighted (T1W) and 123 for T2-weighted (T2W).
LL = Log Likelihood; SE = standard error.

three weeks, thrombus organization appeared more evident with fibrous tissue (i.e., collagen) occupying half of the area and appearance of smooth-muscle cells and neo-vessels (Fig. 5C). At six weeks, the thrombus appeared completely organized showing new vessels and dense collagen matrix, while the cellular content was reduced (Fig. 5D). A similar histologic pattern was seen at nine weeks.

Thrombus size. Cross-sectional thrombus size assessed by MR correlated well with histopathology (Pearson coefficient R = 0.89). Thrombus area measured by MR was 20% to 25% higher than that measured by histology, reflecting shrinkage induced by sample fixation. Intra- and interobserver variability assessment by an intraclass correlation for both MR imaging and histopathology showed good reproducibility, with intraclass correlation coefficients ranging from 0.92 (interobserver) to 0.96 (intraobserver).

DISCUSSION

Magnetic resonance imaging has been used to study atherosclerotic plaques in vivo in humans and in different animal models. We are now reporting the detection and definition of age of arterial thrombi in the carotid artery using MR in a porcine model. We demonstrate that the black-blood MR imaging technique allows the detection and the discrimination between occlusive and mural thrombi. In addition, we demonstrate that the SI of the evolving thrombus shows predictable temporal changes and that the combination of T1W and T2W sequences permits the definition of thrombus age with adequate sensitivity and specificity. The observed MR changes reflect the histologic changes associated with thrombus organization.

MR detection of thrombi. Even though MR imaging has been successfully used in humans for the detection of deep venous thrombosis and definition of their extension (25), its ability to detect arterial thrombi has not been extensively studied. The red cell-rich venous thrombus passes through different predictable stages, which have specific MR relaxation properties that can be used in the diagnosis of deep venous thrombosis. Similar MR properties have been reported in complicated plaques (probably as a consequence of intraplaque hemorrhage) (26) and in intramural hematomas (7). However, the different content and distribution of platelets, fibrin and red cells of arterial and venous thrombi limit the application of similar MR sequences in arterial thrombosis. We decided, therefore, to develop a catheter-based animal model of arterial thrombosis (without external damage to the artery to avoid perivascular MR artifacts) to test the value of high-resolution black-blood MR sequences for serial study of arterial thrombosis. The porcine model has been extensively used for the purposes of atherosclerosis research. The pig carotid artery anatomy and size are similar to those in humans. Consequently, the MR imaging methods and spatial resolution would be comparable for pigs and humans. The imaging sequences and spatial resolution used in this study are currently possible in vivo in humans (27).

Table 2. Sensitivity and Specificity of the Observers in Age Classifications

Age	Sensitivity (%)	Specificity (%)
Acute		
Observer 1	86.7	91.4
Observer 2	100	100
Medium		
Observer 1	86.7	90.7
Observer 2	100	93.0
Old		
Observer 1	89.3	100
Observer 2	89.3	100

Pig model of arterial thrombosis. The validity of the model was reflected in the thrombus composition. The histologic analysis of the fresh thrombus (Fig. 5A) showed a mixed fibrin-platelet rich thrombus, a composition equivalent to human arterial thrombus. At later time points, the organized thrombus showed partial recanalization, reabsorption of the hemoglobin degradation products and, finally, fibrotic transformation (Fig. 5D). These changes are similar to those described in chronic coronary occlusions in humans (28).

The origin of the MR signal in arterial thrombi. Several studies have discussed the origin of the MR signal changes in intracerebral hematoma. Some of these studies focused on the presence of paramagnetic forms of hemoglobin that alters the MR relaxation times. The clot matrix formation and the increase in protein content decrease the MR signal in T2W images. Alterations in intracellular protein concentration may be caused by changes in RBC hydration and by their settling. This may lead to some alterations in the MR signal (29).

The MR SI of arterial thrombi may be different than that found previously in cerebral hematoma due to differences in thrombi composition. In fact, the hemoglobin content and

JACC Vol. 39, No. 8, 2002
April 17, 2002:1366–73

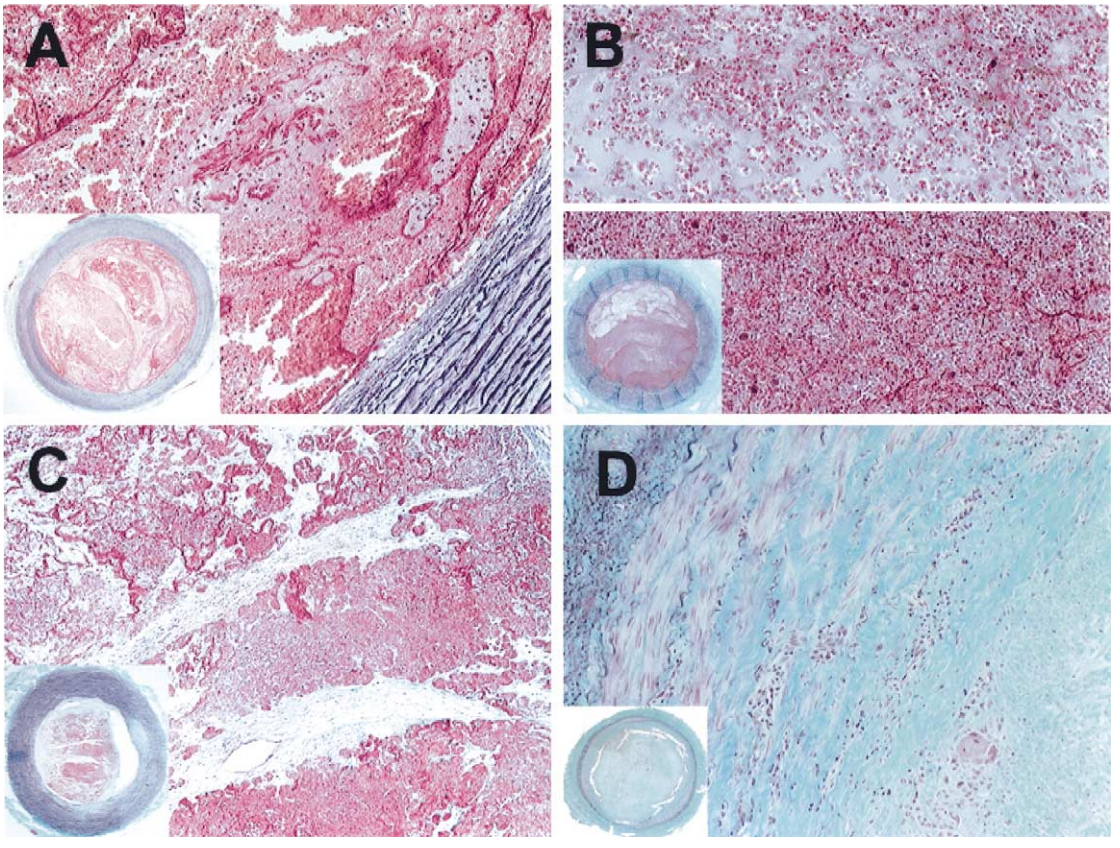

Figure 5. Time-dependent changes of thrombus composition as assessed by light microscopy (combined mason elastin stains). Sections of the thrombotic arteries (20×) and details of the composition (200×) are displayed at different time points: fresh thrombus (≤6 h) **(A)**, one-week-old thrombus **(B)**, three-week-old thrombus **(C)** and six-week-old thrombus **(D).**

its degradation products are lower than those in hematoma or venous thrombi. We speculate that the MR appearance of arterial thrombi and the changes detected over time result from the combination of different oxygenation states of the hemoglobin, changes in intracellular and matrix content of proteins and the hydration of the cellular components. In the few hours after thrombus formation, oxyhemoglobin, a diamagnetic compound, is present within the RBCs so that no shortening of the T1 and T2 relaxation times is expected. This may explain the high signal present in T2W images as well as the intermediate signal of T1W images. At one week, the presence of methemoglobin (short T1 relaxation time) may be responsible for the increase in the signal in T1W images, whereas the high water content of lysed RBCs may explain the high signal in T2W images. Later, the replacement of cellular debris containing methemoglobin by fibrous tissue explains the intermediate SI seen at more than six weeks after thrombus induction.

Translation of the results to human thrombosis. The temporal changes observed in our study may be present at different time points in humans. Most of the SI data were derived from complete occlusive thrombi (as only one animal showed a subocclusive thrombus) and, thus, these observations should not be extrapolated to small mural or mobile thrombi. However, acute coronary syndromes usually occur as a consequence of an occlusive thrombus similar in composition and structure to those induced in our study, rather than from a small mural thrombus.

Future perspective. Further improvements in technique may allow further understanding of the pathobiology of atherothrombosis. In particular, noninvasive in vivo MR could permit tailoring of therapeutic approaches based on thrombus characteristics and help assess treatment efficacy. Magnetic resonance contrast agent targeting active thrombi, such as fresh fibrin (30) or activated platelets, may be useful for the detection of mural thrombi and in the selection of high-risk patients. Improvements in image quality and spatial resolution may provide precise differentiation between thrombus and vessel wall and, therefore, may allow the detection of complicated high-risk plaques even in nonobstructive lesions.

In summary, this study reports on the ability of in vivo MR imaging to detect arterial thrombosis and define the thrombus age. Magnetic resonance allows differentiation between fresh and old thrombi with adequate accuracy using the characteristic visual appearance in T1W and T2W images.

Acknowledgments

The authors thank William F. Chaplin, PhD, for statistical analysis, Bob Guerra and Dr. Hani Jneid for editorial support and Antony Lopez and Jose Rodriguez for helping in the thrombus induction procedures as well as the entire

staff at the Center for Laboratory Animal Sciences for their assistance in the handling and maintenance of the animals.

Reprint requests and correspondence: Dr. Juan J. Badimon, Cardiovascular Biology Research Laboratory, Zena and Michael A. Wiener Cardiovascular Institute, One Gustave L. Levy Place, Box 1030, New York, New York 10029-6574. E-mail: juan.badimon@mssm.edu.

REFERENCES

1. Fuster V, Fayad ZA, Badimon JJ. Acute coronary syndromes: biology. Lancet 1999;353 Suppl 2:SII5–9.
2. Libby P. Current concepts of the pathogenesis of the acute coronary syndromes. Circulation 2001;104:365–72.
3. Wellens HJ. Cardiology: where to go from here? Lancet 1999;354 Suppl:SIV8.
4. Fuster V, Badimon L, Badimon JJ, Chesebro JH. The pathogenesis of coronary artery disease and the acute coronary syndromes. N Engl J Med 1992;326:242–50.
5. Davies MJ, Thomas AC. Plaque fissuring—the cause of acute myocardial infarction, sudden ischaemic death, and crescendo angina. Br Heart J 1985;53:363–73.
6. Virmani R, Kolodgie FD, Burke AP, Farb A, Schwartz SM. Lessons from sudden coronary death: a comprehensive morphological classification scheme for atherosclerotic lesions. Arterioscler Thromb Vasc Biol 2000;20:1262–75.
7. Murray JG, Manisali M, Flamm SD, et al. Intramural hematoma of the thoracic aorta: MR image findings and their prognostic implications. Radiology 1997;204:349–55.
8. Abela GS, Eisenberg JD, Mittleman MA, et al. Detecting and differentiating white from red coronary thrombus by angiography in angina pectoris and in acute myocardial infarction. Am J Cardiol 1999;83:94–7.
9. Feld S, Ganim M, Carell ES, et al. Comparison of angioscopy, intravascular ultrasound imaging and quantitative coronary angiography in predicting clinical outcome after coronary intervention in high risk patients. J Am Coll Cardiol 1996;28:97–105.
10. Fayad ZA, Fuster V. Clinical imaging of the high-risk or vulnerable atherosclerotic plaque. Circ Res 2001;89:305–16.
11. Skinner MP, Yuan C, Mitsumori L, et al. Serial magnetic resonance imaging of experimental atherosclerosis detects lesion fine structure, progression and complications in vivo. Nature Med 1995;1:69–73.
12. Toussaint JF, LaMuraglia GM, Southern JF, Fuster V, Kantor HL. Magnetic resonance images lipid, fibrous, calcified, hemorrhagic, and thrombotic components of human atherosclerosis in vivo. Circulation 1996;94:932–8.
13. Yuan C, Beach KW, Smith LH, Jr., Hatsukami TS. Measurement of atherosclerotic carotid plaque size in vivo using high resolution magnetic resonance imaging. Circulation 1998;98:2666–71.
14. Fayad ZA, Nahar T, Fallon JT, et al. In vivo magnetic resonance evaluation of atherosclerotic plaques in the human thoracic aorta: a comparison with transesophageal echocardiography. Circulation 2000; 101:2503–9.
15. Fayad ZA, Fuster V, Fallon JT, et al. Noninvasive in vivo human coronary artery lumen and wall imaging using black-blood magnetic resonance imaging. Circulation 2000;102:506–10.
16. Helft G, Worthley SG, Fuster V, et al. Atherosclerotic aortic component quantification by noninvasive magnetic resonance imaging: an in vivo study in rabbits. J Am Coll Cardiol 2001;37:1149–54.
17. Corti R, Osende JI, Fuster V, Fayad ZA, Fallon JT, Badimon JJ. Artery dissection and arterial thrombus aging: the role of noninvasive magnetic resonance imaging. Circulation 2001;103:2420–1.
18. Johnstone MT, Botnar RM, Perez AS, et al. In vivo magnetic resonance imaging of experimental thrombosis in a rabbit model. Arterioscler Thromb Vasc Biol 2001;21:1556–60.
19. Totterman S, Francis CW, Foster TH, Brenner B, Marder VJ, Bryant RG. Diagnosis of femoropopliteal venous thrombosis with MR imaging: a comparison of four MR pulse sequences. Am J Roentgenol 1990;154:175–8.
20. Taber KH, Hayman LA, Herrick RC, Kirkpatrick JB. Importance of clot structure in gradient-echo magnetic resonance imaging of hematoma. J Magn Reson Imaging 1996;6:878–83.
21. Badimon JJ, Ortiz AF, Meyer B, et al. Different response to balloon angioplasty of carotid and coronary arteries: effects on acute platelet deposition and intimal thickening. Atherosclerosis 1998;140:307–14.
22. Worthley SG, Helft G, Fuster V, et al. Noninvasive in vivo magnetic resonance imaging of experimental coronary artery lesions in a porcine model. Circulation 2000;101:2956–61.
23. Du YP, Parker DL, Davis WL, Cao G. Reduction of partial-volume artifacts with zero-filled interpolation in three-dimensional MR angiography. J Magn Reson Imaging 1994;4:733–41.
24. Toussaint JF, Southern JF, Fuster V, Kantor HL. Water diffusion properties of human atherosclerosis and thrombosis measured by pulse field gradient nuclear magnetic resonance. Arterioscl Thromb Vasc Biol 1997;17:542–6.
25. Moody AR, Pollock JG, O'Connor AR, Bagnall M. Lower-limb deep venous thrombosis: direct MR imaging of the thrombus. Radiology 1998;209:349–55.
26. Moody AR, Allder S, Lennox G, Gladman J, Fentem P. Direct magnetic resonance imaging of carotid artery thrombus in acute stroke. Lancet 1999;353:122–3.
27. Corti R, Fayad ZA, Fuster V, et al. Effects of lipid-lowering by simvastatin on human atherosclerotic lesions: a longitudinal study by high-resolution, noninvasive magnetic resonance imaging. Circulation 2001;104:249–52.
28. Srivatsa SS, Edwards WD, Boos CM, et al. Histologic correlates of angiographic chronic total coronary artery occlusions: influence of occlusion duration on neovascular channel patterns and intimal plaque composition. J Am Coll Cardiol 1997;29:955–63.
29. Hayman LA, Taber KH, Ford JJ, Bryan RN. Mechanisms of MR signal alteration by acute intracerebral blood: old concepts and new theories. Am J Neuroradiol 1991;12:899–907.
30. Yu X, Song SK, Chen J, et al. High-resolution MRI characterization of human thrombus using a novel fibrin-targeted paramagnetic nanoparticle contrast agent. Magn Reson Med 2000;44:867–72.